Catalysis Today 189 (2012) 83–92

Contents lists available at SciVerse ScienceDirect

Catalysis Today

journal homepage: www.elsevier.com/locate/cattod

Dual role of carbon in the catalytic layers of perovskite/carbon composites for the electrocatalytic oxygen reduction reaction

T. Poux[a], F.S. Napolskiy[a,b], T. Dintzer[a], G. Kéranguéven[a], S. Ya. Istomin[b], G.A. Tsirlina[b], E.V. Antipov[b], E.R. Savinova[a,*]

[a] Laboratoire des Matériaux, Surfaces et Procédés pour la Catalyse, CNRS-UMR 7515, 25 rue Becquerel, 67087 Strasbourg Cedex, France
[b] Faculty of Chemistry, Moscow State University, 119991 Leninskie Gory, Moscow, Russia

ARTICLE INFO

Article history:
Received 21 December 2011
Received in revised form 4 April 2012
Accepted 11 April 2012
Available online 4 June 2012

Keywords:
Oxygen reduction reaction (ORR)
Perovskite
Carbon
Alkaline electrolyte
Rotating disc electrode (RDE)

ABSTRACT

Perovskite oxides are promising materials for the ORR in alkaline media. However, catalytic layers prepared from perovskite powders suffer from high Ohmic losses and low catalyst utilization. An addition of carbon to the catalytic layers greatly improves the performance of the electrodes in the ORR. In this work composite thin film electrodes comprised of a perovskite oxide (either $LaCoO_3$ or $La_{0.8}Sr_{0.2}MnO_3$) and pyrolytic carbon of the Sibunit family were investigated in aqueous 1 M NaOH electrolyte using cyclic voltammetry and rotating disc electrode (RDE) method with the objective to unveil the influence of carbon on the catalyst utilization and on the ORR electrocatalysis. By systematically varying the oxide to carbon ratio we arrive to the conclusion on the dual role of carbon in composite electrodes. On the one hand, it is required to improve the electrical contact between perovskite particles and the current collector, and to ensure maximum utilization of the perovskite surface. On the other hand, carbon plays an active role in the ORR by catalyzing the O_2 reduction to H_2O_2. Composite electrodes catalyze the $4e^-$ ORR in contrast to carbon which is only capable of catalyzing the $2e^-$ reduction. For $LaCoO_3$ composite electrodes, carbon is responsible for the catalysis of the first steps of the ORR, the role of $LaCoO_3$ being largely limited to the hydrogen peroxide decomposition and/or reduction. For $La_{0.8}Sr_{0.2}MnO_3$ composite electrodes, along with the catalysis of the chemical decomposition and/or reduction of H_2O_2 produced on carbon, the perovskite also significantly contributes to the first steps of the ORR. The results of this work suggest that the ORR on the carbon and the oxide components of composite cathodes must be considered as coupled reactions whose contributions cannot be always separated, and that neglecting the contribution of carbon to the ORR electrocatalysis may lead to erroneous values of the catalytic activity of perovskite materials.

1. Introduction

The cathodic oxygen reduction reaction (ORR) is one of the most important processes in energy conversion systems such as fuel cells and metal-air batteries. The sluggish kinetics of the ORR is largely responsible for the voltage losses in proton exchange membrane fuel cells (PEMFC) and other types of low temperature fuel cells [1,2]. Therefore numerous studies are focused today on the development of new electrocatalysts for the ORR [2–4]. During the last decade the research has been mainly focused on the ORR in acid electrolytes due to the rapid development of PEMFCs. However, the advent of anion exchange membranes with high conductivities and satisfactory stabilities has boosted the interest towards the ORR in alkaline media.

The early studies of the ORR in aqueous alkaline electrolytes were performed on metal electrodes and date back to 1960s [5–7]. It was suggested that likewise the ORR in acidic electrolytes, in alkaline media the reaction may either follow a "direct" $4e^-$ (Eq. (1)) or a "series" pathway. The former involves the rupture of the O—O bond at initial steps, while the latter occurs through formation of HO_2^-/H_2O_2[1] (Eq. (2)). The peroxide intermediate can either diffuse away from the electrode, or be further reduced to OH^- in an electrochemical reaction (Eq. (3)). Alternatively, it may decompose into O_2 and H_2O in a chemical reaction (Eq. (4)). It is obvious that each of the equations below comprises a number of elementary steps which are still not fully understood.

$$O_2 + 2H_2O + 4e^- \rightarrow 4OH^- \quad (1)$$

$$O_2 + H_2O + 2e^- \rightarrow HO_2^- + OH^- \quad (2)$$

* Corresponding author. Tel.: +33 03 68 85 27 39; fax: +33 03 68 85 27 61.
E-mail address: Elena.Savinova@unistra.fr (E.R. Savinova).

[1] Depending on the pH; p*K*a (H_2O_2) = 11.7 [8].

0920-5861/$ – see front matter © 2012 Elsevier B.V. All rights reserved.
http://dx.doi.org/10.1016/j.cattod.2012.04.046

$$HO_2^- + H_2O + 2e^- \rightarrow 3OH^- \quad (3)$$

$$H_2O_2 \rightarrow O_2 + 2H_2O \quad (4)$$

In contrast to the ORR in acidic media, which occurs at a reasonable rate only on noble metal electrodes, the ORR in alkaline media is catalyzed by a wider range of materials, including oxides [9–11], and carbon materials [12,13]. It was already clear from the early studies that transition metal oxides can catalyze either the "direct" pathway (Eq. (1)), or the electroreduction of peroxide (Eq. (3)) and/or its decomposition (Eq. (4)). Electrocatalytic activity of oxides in the H_2O_2 reduction (Eq. (3))/decomposition (Eq. (4)) has motivated many researchers to use them for improving the electrocatalysis of the ORR on carbon, typically supporting only the $2e^-$ reaction (Eq. (2)) at reasonable overvoltages [12,13].

In this work, perovskite oxides are studied as the ORR electrocatalysts in alkaline media in view of their potential applications in alkaline fuel cells with solid polymer electrolytes (SAFC). The perovskite structure ABO_3 can incorporate almost any metal cation either in A or in B position thanks to some tolerance to the distortions of the structure [14,15]. Thus, the properties of perovskite-based catalysts can be tuned by varying the composition of oxides, offering vast possibilities for electrocatalysis. Here we focus on $LaCoO_3$ and $La_{0.8}Sr_{0.2}MnO_3$, which have demonstrated high catalytic activity in the ORR and OER (oxygen evolution reaction) [16–19].

Various electrode configurations have been applied to study the ORR/OER electrocatalysis on perovskites, including pellets [16,17,20], gas-diffusion electrodes [21–25], films obtained by painting the oxide slurry on a metal foil [26,27], or by spreading oxide particles and a binder, with or without carbon, on a glassy carbon support [18,28–31]. The thin film approach is compatible with the rotating disc (RDE) [28] and the rotating ring disc electrode (RRDE), the advantage compared to the gas-diffusion electrode consisting in a more reliable separation of kinetic and mass transport contributions. While pellets allow to avoid binders or other additives, their disadvantage lies in the high porosity and concomitant internal diffusion complications. For example, Bockris and Otagawa [32] estimated the roughness factor of perovskite pellets prepared by solid state synthesis as ca. 1000. Moreover, electrode formulations containing perovskites alone usually suffer from high Ohmic losses, posing problems for the ORR investigation but also for practical applications of perovskite materials as fuel cell cathodes.

Addition of carbon powders significantly improves the conductivity of oxide-based electrodes. Several studies have proven that carbon is required in order to increase the electrocatalytic efficiency of oxide materials [23,25]. However, an appreciable catalytic activity of carbon in the ORR in alkaline media brings up a question on the separation of contributions from the two components in these composite materials. Recent studies of the ORR on perovskite oxides neglect the contribution of carbon into the ORR kinetics, even if the latter is added to the thin film electrodes [28,29]. Therefore, the objective of this work is to unveil the role of carbon in perovskite/carbon composite cathodes, and to verify the correctness of conventional approaches to quantify the activity of perovskites by either neglecting or subtracting the contribution of carbon to the ORR kinetics. In order to achieve this goal, we vary systematically the oxide to carbon ratio and study electrochemical and electrocatalytic properties of thin film composite electrodes using cyclic voltammetry and the RDE method. The results of this work suggest that the ORR on the carbon and the oxide components of composite cathodes must be considered as coupled reactions whose contributions cannot be always separated. Thus, either neglecting or subtracting the contribution of carbon to the ORR electrocatalysis may lead to erroneous values of the catalytic activity of perovskite materials.

2. Materials and methods

2.1. Synthesis and characterization

Ceramic samples of $LaCoO_3$ and $La_{0.8}Sr_{0.2}MnO_3$ were synthesized with the sol–gel method described in Ref. [33] using polyacrylamide gel. Samples were annealed in air at 650 °C for 1 h, and milled in a planetary mill in the presence of ethanol for 3 h at 120 rpm using WC balls. The phase purity of compounds was verified by X-ray powder diffraction recorded with Huber G670 Image plate Guinier diffractometer (CuKα1 radiation, curved Ge monochromator, image plate detector). Unit cell parameters were refined by the full profile Rietveld analysis using the GSAS program package [34,35].

The morphology of the samples was analyzed by scanning electron microscopy (SEM), while the elemental distribution of the composite electrodes was studied using the energy-dispersive X-ray spectroscopy (EDX) and the elemental mapping methods (Jeol 6007F). The specific surface area of powders was determined by Brunauer, Emmett and Teller (BET) method (Micromeritics).

2.2. Electrode preparation

In this work, the effect of the quantity of carbon at a constant loading of perovskite (91 $\mu g\ cm_{geo}^{-2}$) and the quantity of perovskite at a constant loading of carbon (37 $\mu g\ cm_{geo}^{-2}$) on the ORR were studied. Carbon of the Sibunit family (BET surface area 65.7 $m^2\,g^{-1}$) was chosen for its high purity, avoiding reactions catalyzed by impurities, and high electrical conductivity [36–38]. The desired amounts of the oxide and carbon powder were mixed together (Table 1). Milli-Q water (18.2 MΩ cm, Purelab) was added to get a desired suspension of the powder: 0.67 $g\,L^{-1}$ of perovskite for the samples with the constant amount of perovskite, and 0.27 $g\,L^{-1}$ of carbon for the samples with the constant amount of carbon. The suspension was then treated in an ultrasonic bath during 30 min to break down agglomerates and disperse particles. A glassy carbon (GC) RDE (0.07 cm^2 geometric area, Autolab) was successively polished with 1.0, 0.3 and 0.05 μm alumina slurry (Escil) to get a mirror finish. 3.2 μL of the catalyst suspension was taken under sonication to keep a homogeneous mixture, drop cast onto the GC support following the procedure adapted from Schmidt et al. [39], and dried under N_2. This last operation – deposition and drying – was repeated three times in order to get a homogeneous coverage of the electrode and to improve the reproducibility. After drying, 2 μL of an alkaline AS-4 ionomer from Tokuyama Company (0.011 wt.% solution in water) was added as a binder to improve the stability of the thin layer electrode. In order to better identify the contribution of carbon, electrodes containing only carbon (no perovskite) and ionomer were prepared following the same procedure and the quantities as indicated in Table 1.

The thickness t of the catalytic layer was estimated using Eq. (5):

$$t = m_1/(\pi r^2 \rho_1) + m_2/(\pi r^2 \rho_2) \quad (5)$$

Here m_1 and m_2 stand for the mass of the perovskite oxide and carbon, respectively; ρ_1 and ρ_2 for the density of the perovskite oxide and carbon, respectively; r is the radius of the RDE (0.15 cm). The powder densities of materials used in this study were estimated as 0.65 and 0.4 $g\,cm^{-3}$ for perovskite oxides and the Sibunit carbon, correspondingly.

Pt/C (40 wt.% Pt on carbon black, Alfa Aesar) was utilized as a benchmark of the ORR activity. The surface area of Pt particles on the electrode was estimated using the coulometry of the hydrogen underpotential deposition and found to be 1.34 cm^2.

Table 1
Loading, surface area and estimated thickness of the electrodes.

	Constant perovskite loading					Constant carbon loading			
Perovskite loading ($\mu g\ cm_{geo}^{-2}$)	91	91	91	91	91	0	46	91	180
Perovskite surface area ($cm^2\ cm_{geo}^{-2}$)									
$LaCoO_3$	9.1	9.1	9.1	9.1	9.1	0	4.6	9.1	18
$La_{0.8}Sr_{0.2}MnO_3$	16	16	16	16	16	0	7.8	16	31
Carbon loading ($\mu g\ cm_{geo}^{-2}$)	0	18	37	140	820	37	37	37	37
Carbon surface area ($cm^2\ cm_{geo}^{-2}$)	0	12	24	90	540	24	24	24	24
Content of perovskite in the composite (wt.%)	100	83	71	40	10	0	56	71	83
Layer thickness (μm)	1.4	1.9	2.3	4.8	22	0.9	1.6	2.3	3.7

2.3. Electrochemical characterization

The electrochemical measurements were performed in a standard three-electrode cell. All parts of the electrochemical cell in contact with the alkaline electrolyte were in Teflon whereas the rest was in Pyrex. 1 M NaOH electrolyte was prepared from an extra pure NaOH solution (Acros Organics, 50 wt.% solution in water) and Milli-Q water (18.2 MΩ cm, Purelab). Since the preparation was performed in air, carbonate impurities cannot be completely excluded. The counter electrode was a platinum wire, and the working electrode was a RDE described in Section 2.2. A Hg/HgO/1 M NaOH electrode (IJ Cambria Scientific) was used as a reference. Its potential was calibrated vs. the reversible hydrogen electrode (RHE) in the same electrolyte and was equal to +0.93 V vs. RHE. In what follows the electrode potentials are given in the RHE scale. The electrolyte resistance as measured by the electrochemical impedance spectroscopy was equal to ca. 15 Ω. No IR correction was applied. All electrochemical measurements were performed using Autolab potentiostat with an analog scan generator at a scan rate of 10 mV s^{-1} at 25 °C. The RDE onto which a thin film of perovskite/carbon composite was applied was immersed in a N_2-purged electrolyte and cyclic voltammetry (CV) measurements were performed until a stable voltammogram was obtained. The latter was then used as a background for the ORR measurements. The potential window was restricted to +0.43 V/+1.23 V vs. RHE in order to avoid the irreversible oxide reduction at more negative, or the carbon oxidation at more positive potentials. Stable voltammograms were observed in this potential range. Then, O_2 was bubbled through the electrolyte for at least 45 min to get a saturated solution, and RDE voltammograms were taken at various rotation speeds of 400, 900, 1600, 2500 rpm. At 10 mV s^{-1} scan rate, the difference of the positive and the negative ORR scans after the background correction (a CV under N_2 atmosphere) was negligible. All experiments were made two or three times, the experimental error of the catalyst deposition on the RDE was estimated to be within 10%.

3. Results and discussion

3.1. Materials characterization

The BET surface area was measured as 10 $m^2\ g^{-1}$ for $LaCoO_3$ and 17 $m^2\ g^{-1}$ for $La_{0.8}Sr_{0.2}MnO_3$. XRD patterns shown in Fig. 1 confirm that $LaCoO_3$ is a single phase compound, and that an admixture of ca. 2 wt.% of WC resulting from the ball milling is present in $La_{0.8}Sr_{0.2}MnO_3$. The unit cell parameters are shown in Table 2.

Table 2
Unit cell parameters of $LaCoO_3$ and $La_{0.8}Sr_{0.2}MnO_3$ obtained by the Rietveld refinement.

Compound	Space group	Unit cell parameters
$LaCoO_3$	R-3c	$a = 5.3852(2)$ Å, $\alpha = 60.678(1)°$
$La_{0.8}Sr_{0.2}MnO_3$	R-3c	$a = 5.4732(1)$ Å, $\alpha = 60.416(2)°$

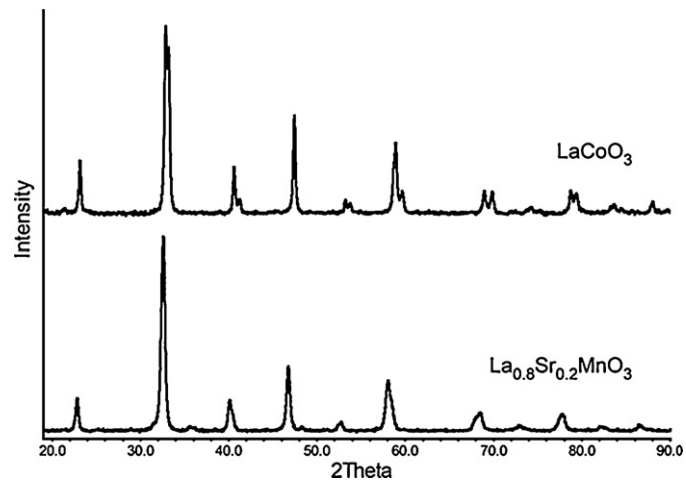

Fig. 1. XRD patterns of $LaCoO_3$ and $La_{0.8}Sr_{0.2}MnO_3$.

SEM analysis revealed that samples consist of μm size agglomerates which comprise nanoparticles with the size around 100 nm. A typical SEM image of the perovskite powder is presented in Fig. 2 for $LaCoO_3$.

In order to explore the morphology of the composite oxide/carbon electrodes they were studied with SEM/EDX. Fig. 3 shows a SEM image, an EDX spectra, and an elemental mapping of $LaCoO_3$/carbon electrode. The SEM image (Fig. 3a) shows agglomerates whose size ranges from several hundred nm to a few μm. The elemental mapping suggests that perovskite and carbon are well intermixed in the catalytic layer and allows to distinguish areas enriched either in perovskite (high Co intensity) or in C. For example, one may notice a perovskite agglomerate (see enclosed area in Fig. 3a) featuring high concentration of Co (Fig. 3d) but impoverished in carbon (Fig. 3c). Although the presence of carbon in the

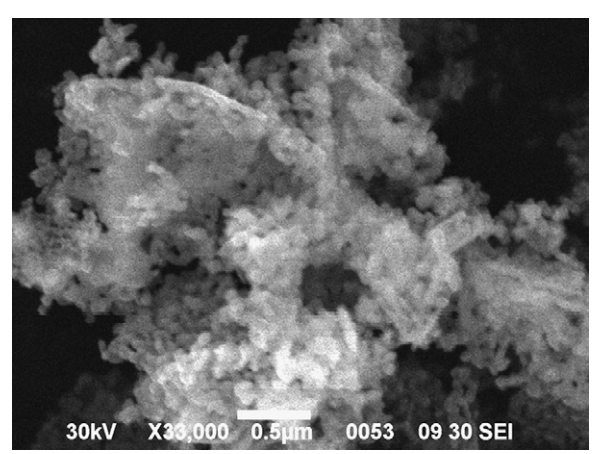

Fig. 2. SEM image of the $LaCoO_3$ powder.

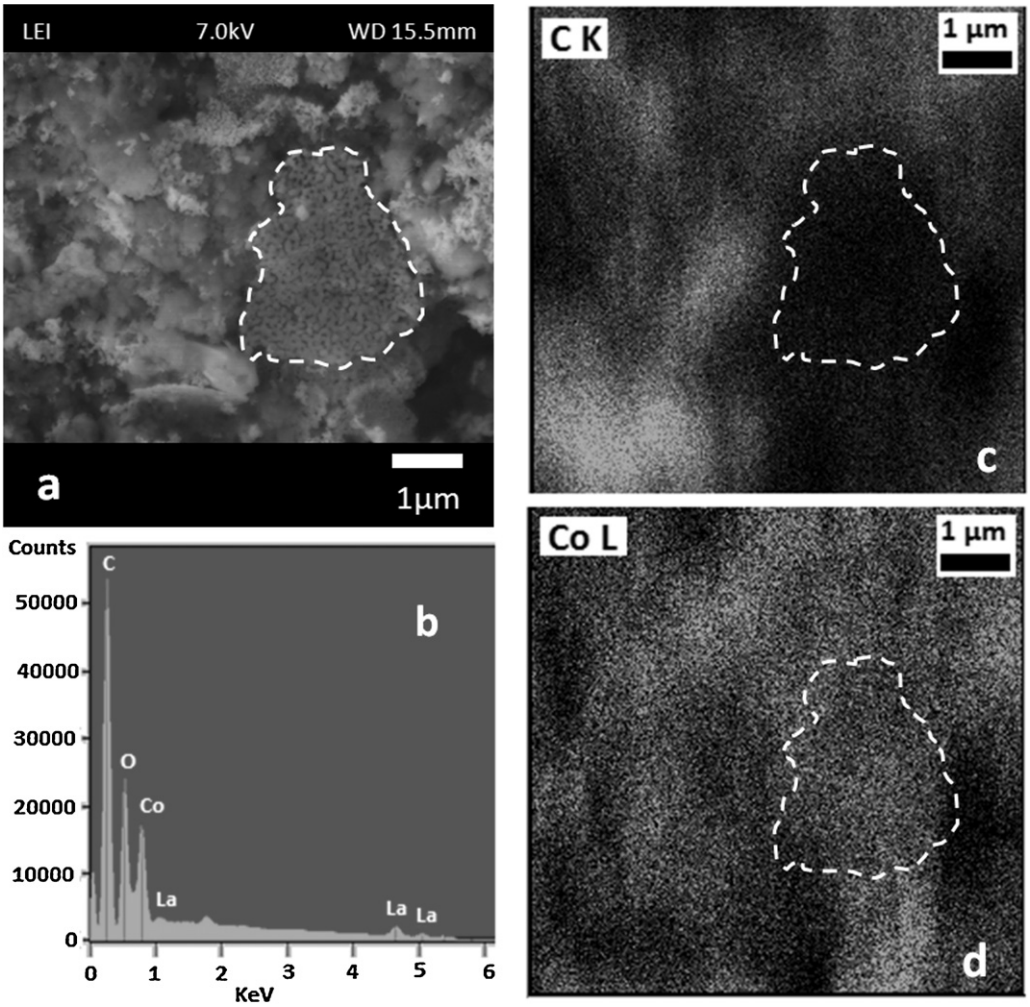

Fig. 3. (a) SEM image, (b) EDX spectrum averaged across the frame, and elemental mapping of (c) C and (d) Co for $LaCoO_3$ + Sibunit composite deposited on a glassy carbon support. Dash line encloses an agglomerate of $LaCoO_3$ particles.

electrode is confirmed by EDX, Sibunit particles could not be clearly visualized and distinguished from the perovskite.

3.2. Cyclic voltammetry of perovskites in supporting electrolyte: influence of carbon

The addition of carbon was found to strongly affect CVs of $LaCoO_3$ and $La_{0.8}Sr_{0.2}MnO_3$ oxides (Fig. S1 in Supplementary data). In order to better visualize the influence of carbon on the measured total capacitance of the electrodes, difference voltammograms were constructed by subtracting the CV of pure carbon from the CV of the composite perovskite/carbon electrode containing the same amount of carbon (Fig. 4). Two effects are observed upon addition of carbon to the thin film electrodes. First, for both oxides the total capacitance increases with the quantity of carbon. One may assume that carbon improves the contact of perovskite particles with the current collector and thus allows higher utilization of their surface. Second, the difference between the anodic and the cathodic peak potentials shrinks, suggesting that the addition of carbon decreases the Ohmic resistance of the layer. For $La_{0.8}Sr_{0.2}MnO_3$, the total capacitance seems to level off around 37 $\mu g\ cm^{-2}_{geo}$ of carbon, whereas, for $LaCoO_3$, it keeps increasing. The difference observed between two oxides is in agreement with the higher intrinsic conductivity of $La_{0.8}Sr_{0.2}MnO_3$ (43 $S\,cm^{-1}$ at 25 °C [40]) compared with $LaCoO_3$ (1.5 $S\,cm^{-1}$ at 25 °C [41]). This is due to the Sr doping of $La_{0.8}Sr_{0.2}MnO_3$ which insures the presence of electronic and ionic defects, leading to an increased conductivity of the perovskite [42,43].

CVs in supporting electrolyte confirm that, in agreement with the literature data [23,25], carbon is indeed required for improving the quality of the thin film oxide electrodes. Although intrinsic conductivities of $LaCoO_3$ and $La_{0.8}Sr_{0.2}MnO_3$ are relatively high, the Ohmic resistance of compacted perovskite powders is dominated by the contact resistance between particles. Addition of carbon allows "wiring" oxide particles and improving particle–particle as well as particle–current collector electrical contact. This leads to a strong decrease of the Ohmic resistance and an enhancement of the surface utilization. For example, for $LaCoO_3$ redox peaks shift by more than 100 mV upon carbon addition. For currents on sub-mA level (0.01 $mA\,cm^{-2} \times 0.07\,cm^2$) this suggests a layer resistance above 100 kΩ. Simultaneously, the total capacitance increases by more than a factor of 2 suggesting ca. 2 times higher utilization of the perovskite surface. Note however that some type of oxygen spillover from the oxide to the carbon surface, similar to what has been earlier reported in Ref. [9], cannot be fully excluded. The improvement of the oxide layer conductivity is expected to affect its measured catalytic activity in the ORR, which will be discussed in the next section.

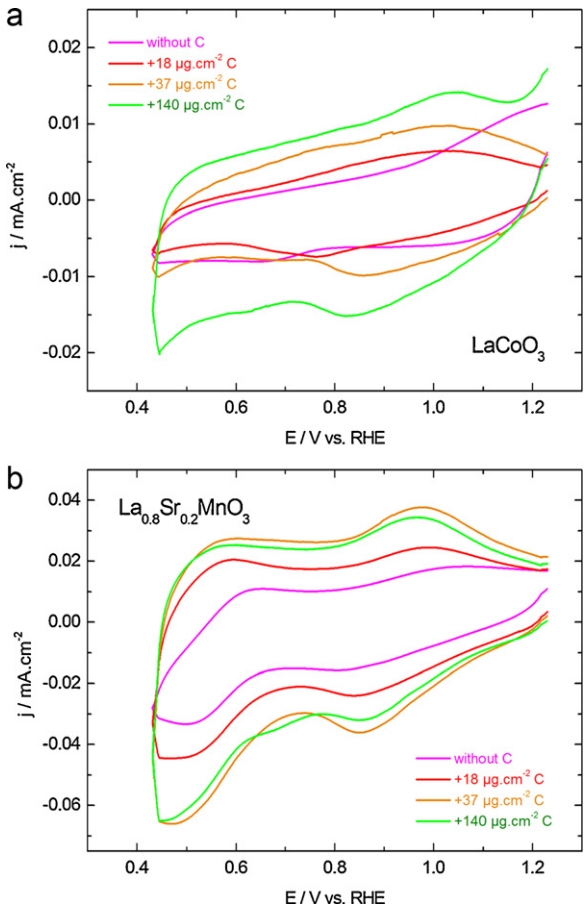

Fig. 4. Difference voltammograms obtained by subtracting CVs of Sibunit (Fig. S1a) from corresponding CVs of perovskite/Sibunit composite electrodes (Fig. S1b and c) in N_2-purged 1 M NaOH at 10 mV s^{-1} for $LaCoO_3$ (a) and $La_{0.8}Sr_{0.2}MnO_3$ (b). Measurements were performed with a constant amount of perovskite (91 μg cm^{-2}_{geo}) and variable amount of carbon. Color codes: 0 (pink), 18 (red), 37 (orange) and 140 μg cm^{-2}_{geo} (green). Currents are normalized to the geometric area of the electrode. (For interpretation of the references to color in this figure legend, the reader is referred to the web version of the article.)

3.3. Rotating-disk electrode study of the ORR on perovskite/carbon composites: influence of carbon and perovskite loadings

The ORR activity of $LaCoO_3$ and $La_{0.8}Sr_{0.2}MnO_3$ oxides was studied with various quantities of carbon (Table 1) and compared with the activity of GC, Pt/C, and electrodes containing variable amounts of carbon using the RDE. Fig. 5b and c indicate that electrodes containing perovskites without carbon show very low onset potentials, and ORR currents not reaching the diffusion limiting plateau. This is especially true for $LaCoO_3$ whose onset potential is close to that of glassy carbon. For $La_{0.8}Sr_{0.2}MnO_3$, similar RDE data were observed by Tulloch and Donne [18] who did not add carbon to the electrode layer. One may see that addition of carbon strongly increases the activity of the perovskite thin film electrodes which shows up in a systematic shift of the RDE voltammograms towards positive potentials, and an increase in the absolute value of the limiting current. The evolution of voltammograms is similar for composite and for pure carbon electrodes (Fig. 5a). Hence, we start the discussion with the analysis of the ORR data for GC and for carbon film electrodes. This will then help in the understanding of the results for perovskite/carbon composites.

For the GC electrode, one may notice a particular shape of the RDE voltammogram which shows a broad maximum around 0.55 V vs. RHE and, as discussed below, does not attain the diffusion limiting current in the potential window studied. This was also observed by Tammeveski et al. [44] and explained by the surface functional group mediated oxygen reduction to hydrogen peroxide. The most active sites responsible for the positive onset of the ORR and the maximum in the RDE are limited in number, and were attributed to quinone groups. The RDE shape was quantitatively

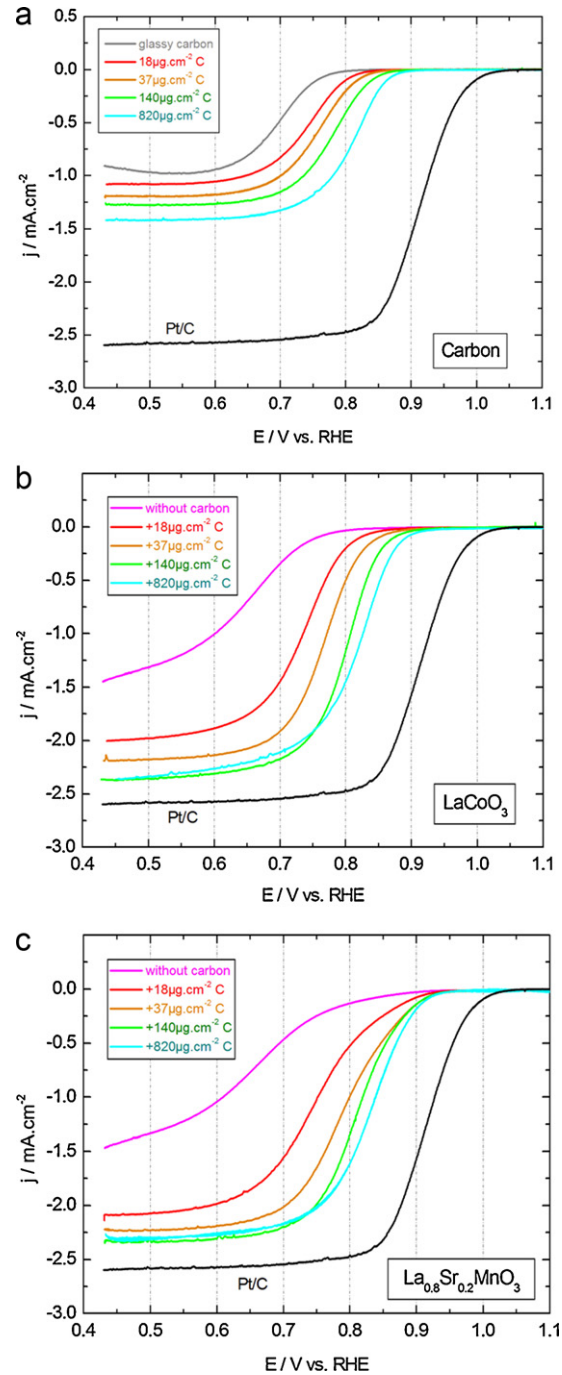

Fig. 5. Positive scans of the RDE voltammograms of GC-supported thin films of carbon Sibunit (a), $LaCoO_3$ + Sibunit (b), and $La_{0.8}Sr_{0.2}MnO_3$ + Sibunit (c) in O_2-saturated 1 M NaOH at 900 rpm and 10 mV s^{-1}. Measurements were performed with a constant amount of perovskite (91 μg cm^{-2}_{geo}) for (b) and (c), and variable amount of carbon. Color codes: 0 (pink), 18 (red), 37 (orange), 140 (green) and 820 μg cm^{-2}_{geo} (light blue). Grey and black lines show RDE curves for GC and Pt/C, respectively. Currents are normalized to the geometric area of the working electrode and corrected to the background currents measured in the N_2 atmosphere. (For interpretation of the references to color in this figure legend, the reader is referred to the web version of the article.)

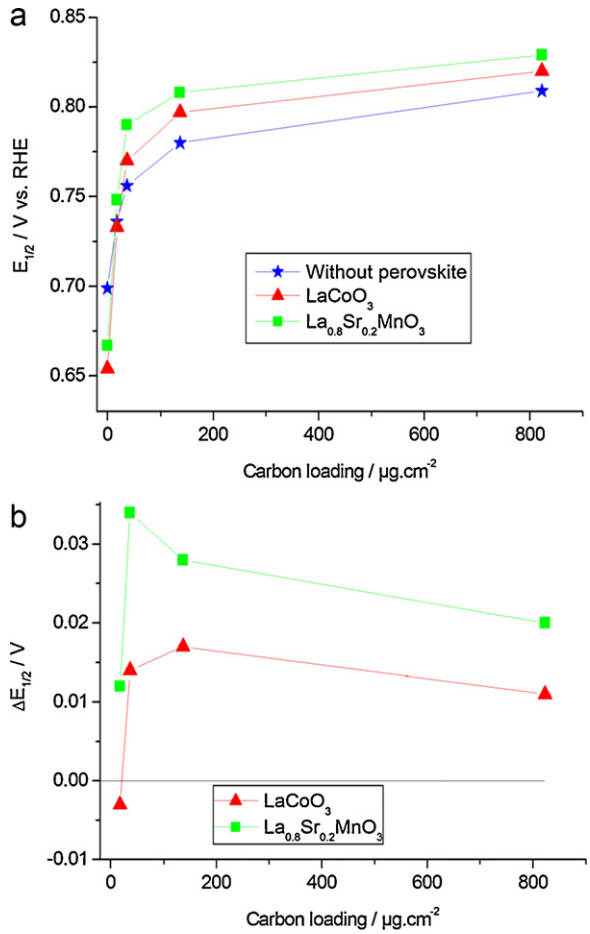

Fig. 6. (a) The ORR half-wave potential $E_{1/2}$ and (b) the difference of the half-wave potential $\Delta E_{1/2}$ between perovskite/carbon and pure carbon electrodes vs. the carbon loading, in O_2-saturated 1 M NaOH. Blue stars represent pure carbon electrodes, red triangles – electrodes with 91 µg cm^{-2}_{geo} of $LaCoO_3$ and carbon Sibunit, and green squares – electrodes with 91 µg cm^{-2}_{geo} of $La_{0.8}Sr_{0.2}MnO_3$ and carbon Sibunit. (For interpretation of the references to color in this figure legend, the reader is referred to the web version of the article.)

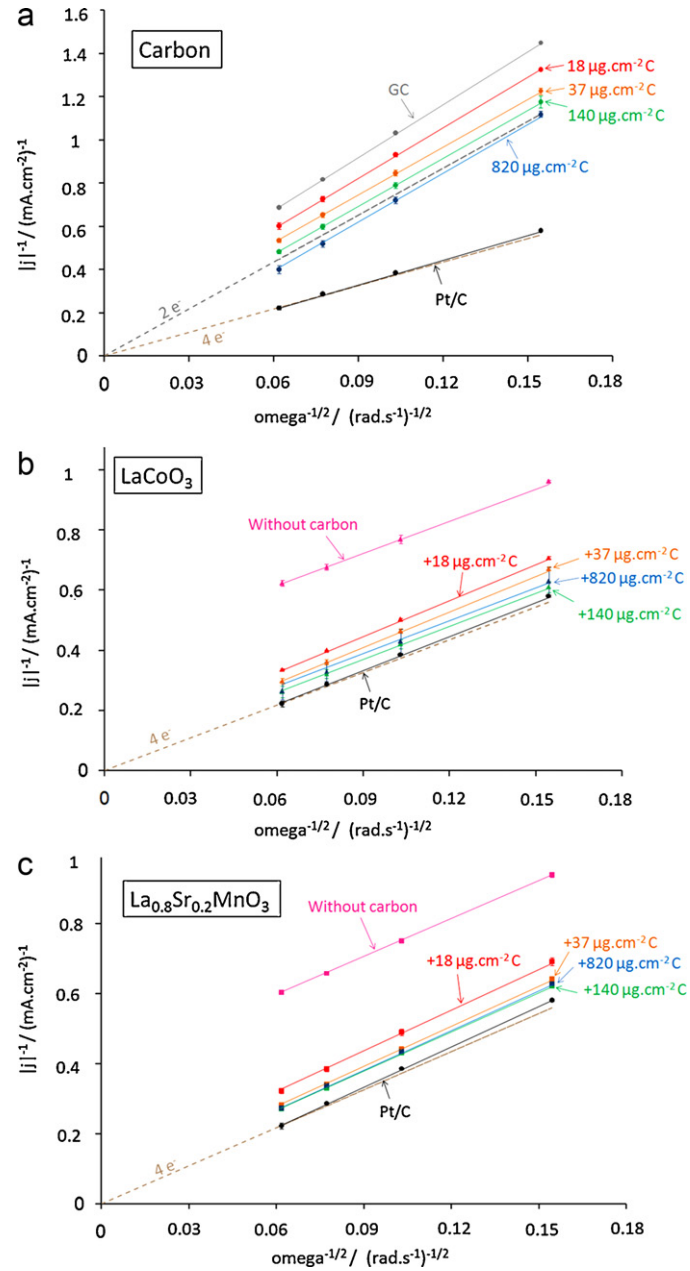

Fig. 7. Koutecky–Levich plots of the ORR current measured at +0.5 V vs. RHE by thin layer RDE method in O_2 saturated 1 M NaOH at 10 mV s^{-1} for carbon Sibunit (a), $LaCoO_3$ + Sibunit (b) and $La_{0.8}Sr_{0.2}MnO_3$ + Sibunit (c). Measurements were performed with a constant amount of perovskite (91 µg cm^{-2}_{geo}) for (b) and (c), and variable amount of carbon. Color codes: 0 (pink), 18 (red), 37 (orange), 140 (green) and 820 µg cm^{-2}_{geo} (light blue). Grey and black symbols stand for GC and Pt/C electrodes, respectively. Dotted lines represent theoretical current values for 2 and 4 electrons in 1 M NaOH at 25 °C. Currents are normalized to the geometric area of the electrode and corrected to the background currents measured in N_2 atmosphere. Error bars represent standard deviation from at least two independent repeated measurements. (For interpretation of the references to color in this figure legend, the reader is referred to the web version of the article.)

modeled [44] within an EC mechanism with the first step being reversible reduction of quinone to semiquinone surface groups. The latter chemically react with molecular oxygen to form superoxide radical which gives rise to HO_2^- either in a chemical or in an electrochemical consecutive step. The onset and the shape of the RDE voltammogram thus depend on the type and the red-ox potential of active surface groups on the GC surface.

When a carbon film is deposited on the GC electrode, the RDE curve shifts positive as expected due to the increase of the active surface area (see Table 1). An increase of the amount of carbon results in a systematic positive shift of the ORR onset and the half-wave potential $E_{1/2}$ (Fig. 6) and an increase of the absolute value of the limiting current. The RDE voltammograms of carbon electrodes and their positive shift with an increasing amount of carbon are in agreement with the well-known fact that carbon materials are active catalysts of the ORR in alkaline media [12,13]. Fig. 7a shows the Koutecky–Levich plots of the limiting currents for GC and for carbon film electrodes with various loadings. For the highest carbon loading of 820 µg cm^{-2}_{geo} the measured limiting current is in reasonable agreement with the theoretical value calculated using the Levich equation (Eq. (6)):

$$I = -0.62AnFD_{O_2}^{2/3}\nu^{-1/6}C_{O_2}\omega^{1/2} \quad (6)$$

for the following parameter values [13]: the concentration of O_2 in the saturated 1 M NaOH electrolyte at 25 °C, $C_{O_2} = 8.4 \times 10^{-7}$ mol cm^{-3}, the diffusion coefficient $D_{O_2} = 1.64 \times 10^{-5}$ cm^2 s^{-1}, the kinematic viscosity $\nu = 0.011$ cm^2 s^{-1}, the number of electrons $n = 2$, and the geometric surface area $A = 0.07$ cm^2. This is in agreement with the current understanding of the ORR on carbon electrodes which in the investigated

potential interval predominantly proceeds to hydrogen peroxide [12,13,44].

It should be noted however that nonzero *y* intercepts are observed for carbon and composite electrodes with carbon loading below 820 $\mu g\ cm_{geo}^{-2}$ as well as for GC (Fig. 7). Various reasons can be proposed to account for this phenomenon, namely (i) an inhomogeneity of the catalyst distribution on the current collector, (ii) a diffusion resistance in the ionomer film [30,45], (iii) an O_2 concentration gradient within a thick catalyst film [46], or (iv) a limited number of active sites leading to the adsorption limitation [46,47]. The linearity of Koutecky–Levich plots insures that the characteristic size of eventual inhomogeneities of the electrode layers is inferior to the thickness of the diffusion layer, which allows to discard the first hypothesis. The apparent thickness of the ionomer film in this work was estimated as ca. 15 nm, which makes the second hypothesis very unlikely. The third option does not seem realistic either since the intercept drops down with the thickness of the film. Finally, the most likely explanation of the nonzero *y* intercept decreasing with the film thickness is a limited number of active sites on the carbon surface. As the loading of carbon increases, the number of active sites increases as well, and the current attains the diffusion limiting value determined by the Levich equation. This explanation is also in agreement with the data for GC reported in this work as well as in the literature [44].

We now turn to the discussion of the ORR on $LaCoO_3$ and $La_{0.8}Sr_{0.2}MnO_3$ oxides. The most striking influence of the addition of perovskites to carbon is the increase of the absolute value of the limiting current, which for oxide/carbon composites approaches the value observed for Pt/C electrode and corresponding to the transfer of $4e^-$. The slopes of Koutecky–Levich plots (Fig. 7b and c) for oxide-based electrodes confirm transfer of $4e^-$ in the overall reaction. Contrary to carbon materials, transition metal oxides, and perovskites in particular, are known to be active catalysts of the catalytic hydrogen peroxide decomposition [48–50], as well as its electrocatalytic reduction [51]. In addition, perovskites may also be active in the first steps of the ORR by activating the O_2 molecule and catalyzing its transformation into OH^- either via a "series" H_2O_2 route or via the so-called "direct" $4e^-$ pathway occurring through O_2/O_2^- splitting [18,29,51]. In order to better understand the observed behavior, we compare the evolution of the half-wave potential $E_{1/2}$ for composite electrodes and for the electrodes containing carbon alone. Fig. 6 shows $E_{1/2}$ and the difference of $E_{1/2}$ ($\Delta E_{1/2}$) between composites and pure carbon electrodes, vs. the carbon loading. First of all, these results indicate that $La_{0.8}Sr_{0.2}MnO_3$ has a higher mass activity in the ORR compared to $LaCoO_3$. Then, it can be observed that both perovskites present higher half-wave potentials than carbon alone, but the evolution with the carbon quantity is similar to that observed for pure carbon. Moreover, while the maximum difference of $E_{1/2}$ for pure perovskites and composite electrodes amounts to more than 250 mV, the difference between $E_{1/2}$ for pure carbon and composites reaches at most 37 mV for $La_{0.8}Sr_{0.2}MnO_3$ and 18 mV for $LaCoO_3$. This confirms that the carbon contribution to the ORR on composite perovskite/carbon electrodes cannot be neglected.

In order to better understand the role of perovskite oxides in the ORR, electrodes with a constant amount of carbon and various quantities of perovskites were studied (Fig. 8). The results displayed in Fig. 8a suggest that an addition of $LaCoO_3$ 46 $\mu g\ cm_{geo}^{-2}$ to the carbon electrode results in doubling the ORR current in the kinetic and mixed region, while further increase of the $LaCoO_3$ loading to 91 and then 180 $\mu g\ cm_{geo}^{-2}$ leads to a marginal increase of the current in the kinetic and mixed region. Such a behavior is consistent with an increase of the rate constant of the chemical disproportionation step as shown by the modeling work of Jaouen [52]. The catalytic activity of perovskites in the H_2O_2 disproportionation has been demonstrated in numerous publications [48–50]. One

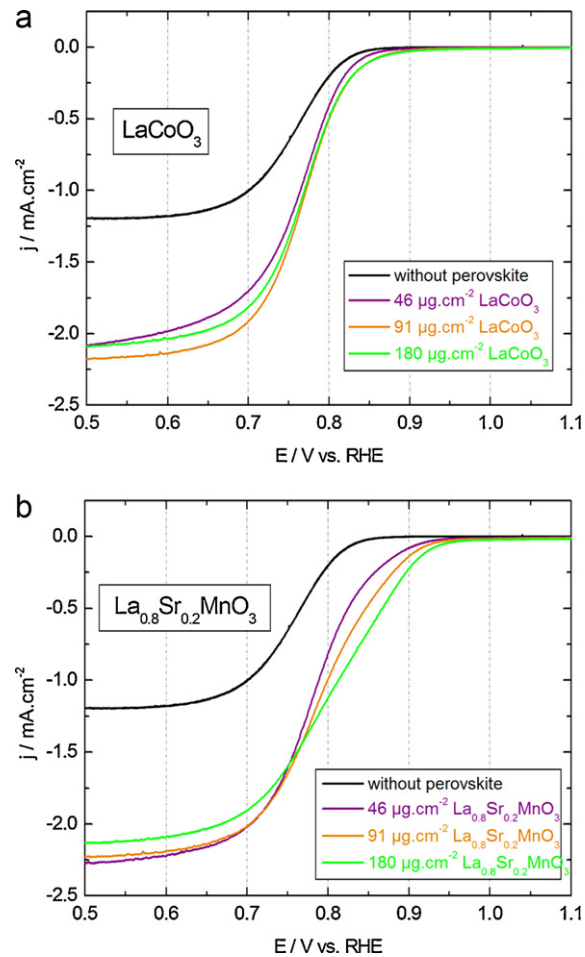

Fig. 8. Positive scans of the RDE voltammograms of GC-supported thin films of $LaCoO_3$ + Sibunit (a), and $La_{0.8}Sr_{0.2}MnO_3$ + Sibunit (b) in O_2-saturated 1 M NaOH at 900 rpm and 10 mV s^{-1}. Measurements were performed with a constant amount of carbon (37 $\mu g\ cm_{geo}^{-2}$) and variable amount of perovskite. Color codes: 0 (black), 46 (purple), 91 (orange), 180 $\mu g\ cm_{geo}^{-2}$ (green). Currents are normalized to the geometric area of the electrode and corrected to the background currents measured in N_2 atmosphere. (For interpretation of the references to color in this figure legend, the reader is referred to the web version of the article.)

should note however that the same effect is expected if $LaCoO_3$ were active in the electrochemical H_2O_2 reduction (Eq. (3)). This suggests that once H_2O_2 is produced on the carbon component of a composite electrode, the role of $LaCoO_3$ is largely reduced to the catalysis of H_2O_2 transformations, either in the chemical disproportionation (Eq. (4)) or the electrochemical reduction reaction (Eq. (3)). More detailed mechanistic studies are required to differentiate between these possibilities. Therefore, for $LaCoO_3$/carbon composites, the first steps of the ORR are mainly electrocatalyzed by carbon. This is in part due to the lower specific surface area of $LaCoO_3$ compared to carbon, and in part due to its fairly low specific electrocatalytic activity [16,53]. The composite electrode may thus be considered as a bifunctional catalyst with carbon catalyzing the ORR into H_2O_2, and perovskite catalyzing further H_2O_2 chemical/electrochemical transformations. Ultimately, O_2 on a composite electrode is reduced to H_2O, while carbon alone is only capable to support the reduction to H_2O_2. Similar role was proposed for MnOOH [54], and for $La_{0.6}Ca_{0.4}CoO_3$ [26,30] in oxide/carbon composite electrodes.

For $La_{0.8}Sr_{0.2}MnO_3$ the behavior is quite different. The RDE curve is shifted more positive compared to the one for $LaCoO_3$, and the increase of the amount of perovskite has a pronounced influence on the ORR onset and on the shape of the RDE curves. Similar

behavior was observed for $LaMnO_3$ [21,22] and for $La_{0.6}Sr_{0.4}CoO_3$ [23]. This may be attributed to the contribution of $La_{0.8}Sr_{0.2}MnO_3$ to the first steps of the ORR. Such a hypothesis is in agreement with the work of Tulloch [18] where $La_{0.8}Sr_{0.2}MnO_3$ electrode without carbon showed significant ORR activity. The exact mechanism of the ORR being beyond the scope of this work, it should be noted however that a mechanism consisting of a *reversible* electrochemical reaction occurring on the surface of carbon (like the above discussed quinine-semiquinone transformation), with a consecutive chemical reaction of H_2O_2 formation, also on the surface of carbon, then followed by a chemical disproportionation of H_2O_2 or its electrochemical reduction on the perovskite surface, would also be consistent with the observed experimental data.

3.4. How to calculate the intrinsic electrocatalytic activity of perovskites in perovskite/carbon composite electrodes

The above discussion shows that carbon actively participates in the ORR on perovskite/carbon composites, the latter acting as bifunctional electrocatalysts. Thus, the ORR on the carbon and the oxide components must be considered as coupled reactions. Depending on the catalytic activity of perovskite materials in various steps of the multistep ORR mechanism, different mechanisms may be expected. This poses problems for the evaluation of the intrinsic electrocatalytic activity of perovskites. In the literature the participation of carbon in the ORR on perovskite/carbon composites is often neglected [28,29], the specific ORR activity being calculated by normalizing the kinetic current to the surface area of a perovskite material. However, this work demonstrates that the contribution of carbon to the ORR cannot be neglected.

In case of a minor coupling of reactions on oxide and on carbon, the contribution of the latter could be accounted for by subtracting the ORR current measured on pure carbon electrodes. In order to elucidate the applicability of such an approach to carbon/perovskite composites we employed the following procedure. In the first place, kinetic currents were calculated by performing the mass transport correction by using Eq. (7):

$$|I|^{-1} = |I_D|^{-1} + |I_K^{p+c}|^{-1} \quad (7)$$

with I is the ORR current, obtained from capacity-corrected positive-going RDE scans, I_D the diffusion limited current, and I_K the kinetic current. Considering that diffusion limited currents are accessible only for some samples, the theoretical values of I_D (normalized to the geometric surface area) of 2.71 and 1.36 mA cm_{geo}^{-2} were applied for the four and two electron reaction, respectively. Then, the current density of the ORR on perovskites j_K^p was calculated by using Eq. (8):

$$j_K^p = \frac{I_K^{p+c} - I_K^c}{A_{BET}^p} \quad (8)$$

Here I_K^{p+c} is the kinetic current of perovskite/carbon composite determined using Eq. (7), I_K^c is the corresponding kinetic current of carbon alone determined for the same quantity of carbon, and A_{BET}^p is the surface area of perovskite calculated from the BET data.

Tafel plots calculated with the said procedure for composites and Tafel plots for pure carbon normalized to the carbon surface area are presented in Fig. 9 (Fig. S2 represents Tafel plots for composites with constant amount of carbon and variable amounts of perovskites). It can be observed that Tafel plots for carbon in the interval of loadings from 18 to 140 μg cm_{geo}^{-2} are almost superposed (Fig. 9a). Glassy carbon shows slightly higher kinetic current densities, which is probably due to an underestimation of its active surface area that was assumed to be equal to the geometric area. The electrode with the highest amount of carbon presents slightly

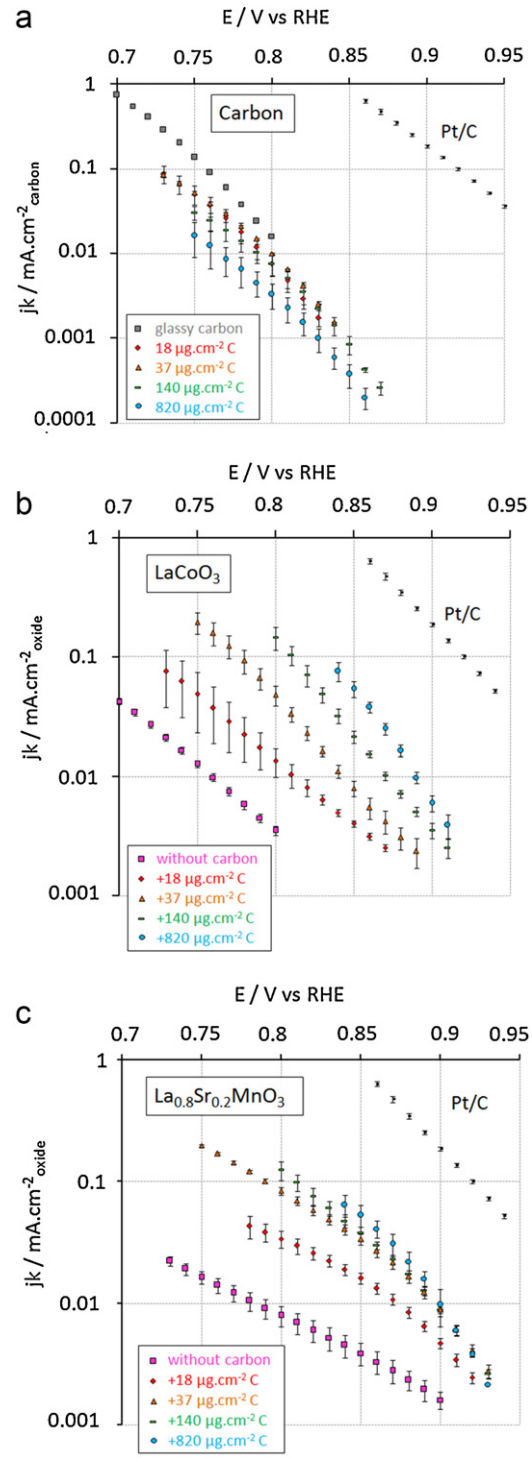

Fig. 9. Tafel plots from mass-transport corrected positive-going scans of GC-supported thin film RDEs in O_2-saturated 1 M NaOH at 10 mV s^{-1}. (a) Sibunit carbon, (b) $LaCoO_3$ + Sibunit, (c) $La_{0.8}Sr_{0.2}MnO_3$ + Sibunit. Measurements were performed with a constant amount of perovskite (91 μg cm_{geo}^{-2}) for (b) and (c) and variable amount of carbon. Color codes: 0 (pink squares), 18 (red diamonds), 37 (orange triangles), 140 (green rectangles) and 820 μg cm_{geo}^{-2} (light blue circles). Grey symbols stand for the GC electrode, while black for the Pt/C electrode. Error bars represent standard deviation from at least two independent repeated measurements. Currents are normalized to the BET surface area of carbon for carbon electrodes, to the BET surface area of perovskites after subtraction of the kinetic ORR current on carbon for composite electrodes, to the platinum surface area for Pt/C, and to the geometric surface area for GC. (For interpretation of the references to color in this figure legend, the reader is referred to the web version of the article.)

lower current densities than other carbon electrodes. This underestimation can be explained by Eq. (9):

$$I_K = j_K \cdot A_{real} \cdot u_f \quad (9)$$

with j_K is the kinetic current density, A_{real}, the real surface area, and u_f the utilization factor, which accounts for the mass-transport or Ohmic hindrance in the layer. For thin layers, the utilization factor equals 1. For thick layers however, it is inferior of 1, due to the mass transport hindrance of oxygen molecules within the catalytic layer [46,55].

For $LaCoO_3$, Tafel plots with various amounts of carbon are not superposed (Fig. 9b). Indeed, it is observed that the higher the quantity of carbon added to the composite electrode, the higher is the kinetic current density. It is instructive to compare the degree of the kinetic current enhancement with the increase of the total capacitance discussed in Section 3.2. For example, an increase of the amount of carbon from 18 to 140 $\mu g\ cm^{-2}_{geo}$ leads to ca. factor of 2 enhancement of the total capacitance and ca. factor of 10 increase of the kinetic current. In agreement with the discussion above this confirms that the role of carbon extends beyond the improvement of the layer conductivity, and involves also its active participation in the mechanism of the catalytic ORR reduction. This suggests that subtracting the ORR current in the absence of perovskite (Eq. (8)) does not allow to properly account for the carbon contribution.

In the case of $La_{0.8}Sr_{0.2}MnO_3$, for electrodes containing more than 29% of carbon, Tafel plots are almost superposed confirming on the one hand that this amount of carbon is sufficient to achieve a good electrical contact between $La_{0.8}Sr_{0.2}MnO_3$ particles, and on the other hand that the catalytic activity of this perovskite material in the electrochemical ORR is much superior of that of carbon. For each electrode composition, $La_{0.8}Sr_{0.2}MnO_3$ is more active than $LaCoO_3$, as seen in Section 3.3. It should be also noted that $La_{0.8}Sr_{0.2}MnO_3$ demonstrates more pronounced voltammetric peaks, compared to $LaCoO_3$, in the potential interval of interest (these are seen in the CVs under N_2 atmosphere), so its higher activity may be due to a redox mediation mechanism. Since the nature of the peaks is not fully understood yet, such a hypothesis however requires additional studies.

At the typical benchmark condition of 0.9 V vs. RHE [2], and for an electrode containing 60% of carbon, the current density is 3.3 and 8.6 $\mu A\ cm^{-2}_{oxide}$ for $LaCoO_3$ and $La_{0.8}Sr_{0.2}MnO_3$, correspondingly. Without carbon, the current density at 0.9 V vs. RHE is 1.6 $\mu A\ cm^{-2}_{oxide}$ for $La_{0.8}Sr_{0.2}MnO_3$, while Bockris and Otagawa [17] found around 0.1 $\mu A\ cm^{-2}_{oxide}$ for $LaCoO_3$ and $La_{1-x}Sr_xMnO_3$ pellets (~0.1 $mA\ cm^{-2}_{electrode}$ with a reported roughness factor ~1000 $cm^2_{oxide}\ cm^{-2}_{electrode}$). Differences are probably related to the Ohmic resistance and to the mass transport losses in the pellets, and show that the thin film approach based on the application of oxide/carbon composite layers leads to a better utilization of the surface of oxide particles.

One may notice that the ORR activities of composite electrodes are still inferior to the activity of the state of the art Pt/C catalyst, the latter reaching 190 $\mu A\ cm^{-2}_{Pt}$ at 0.9 V vs. RHE (Fig. 9). It should be noted however that as opposed to the noble metal loading, which is constrained by the cost considerations, the loading of non-precious metal oxide catalysts is limited only by the thickness constraints because of the decline of the utilization factor caused by ohmic and mass transport limitations in thick layers [2,28]. Thus, to compensate for the lower specific activity one may envisage higher loadings of metal oxide catalysts. Moreover, it is expected that fine tuning of the perovskite composition will in the future allow to significantly increase the specific activity of this promising class of materials [29].

Convergence of Tafel plots for $La_{0.8}Sr_{0.2}MnO_3$ at high carbon loadings indicates that Eq. (8) may be applied for estimating the intrinsic catalytic activity of this oxide material for a certain range of carbon/perovskite ratios. We would like to stress however that this conclusion cannot be generalized to all types of perovskite/carbon composite electrodes since as discussed above a mechanism consisting of carbon catalyzed formation of H_2O_2 in a reversible electrochemical reaction followed by a perovskite catalyzed H_2O_2 transformations would also be able to account for a significant positive shift of the onset of the ORR even if the oxide were inactive in the ORR electrocatalysis.

4. Conclusions and outlook

This work shows that carbon is required in the catalytic layers containing perovskite oxides in order to achieve high ORR activity. Carbon in the catalytic layer plays a dual role. On the one hand, it is required to improve the electrical contact between perovskite particles and the current collector, and ensure maximum utilization of the perovskite surface. On the other hand, carbon plays an active role in the ORR by catalyzing O_2 reduction to H_2O_2. The ORR on the carbon and the oxide components of composite cathodes must be considered as coupled reactions whose contributions cannot be always separated. Depending on the type and the surface area of perovskite and of carbon, but also on the electronic conductivity of the perovskite material, carbon may fully take over the catalytic role of the electrochemical O_2 activation. In such a case the role of perovskite is reduced to either chemical disproportionation or electrochemical reduction of H_2O_2. Then, calculation of the electrocatalytic activity by normalizing the measured kinetic current to the surface area of perovskite (with or without subtraction of the carbon contribution) will lead to erroneous results. This is more pronounced for $LaCoO_3$ than for $La_{0.8}Sr_{0.2}MnO_3$ in this work.

The quantity (and presumably the type) of carbon in the composite electrodes must be carefully selected in order to ensure the highest catalytic activity of the composite and depends on the intrinsic conductivity of an oxide, and presumably the size of oxide particles.

Thus, further development of perovskite materials for SAFCs should go along with the understanding of the mutual influence of perovskite and carbon in the catalytic layer and an improvement of the composition and morphology of carbon/perovskite composites. This also requires the understanding of the ORR on composite electrodes and of the participation of carbon and perovskite materials in chemical and electrochemical steps of the O_2 activation, H_2O_2 reduction and decomposition. At present the available information is not sufficient to conclude on the "direct" $4e^-$ vs. the "series" $2e^- + 2e^-$ ORR on perovskite materials. Further detailed RRDE studies of the ORR, as well as investigations of the H_2O_2 chemical/electrochemical reactions on perovskites are required.

Note that the ORR on carbon materials cannot be fully neglected even if perovskite materials are highly active in the "direct" $4e^-$ ORR. Indeed, if carbon is eventually part of the cathode layer of a SAFC, H_2O_2 produced on its surface must be either decomposed or further reduced in order to prevent corrosion of the electrode layer and the membrane. Thus, along with the ORR activity, perovskites must possess significant activity in the H_2O_2 reduction or disproportionation.

Acknowledgments

The authors thank P.A. Simonov from the Boreskov Institute of Catalysis of the Russian Academy of Sciences for providing carbon of the Sibunit family, and Tokuyama Company for providing the alkaline ionomer. They are also grateful to P. Bernhardt, A. Rach, and S. Sall for their technical help, and MaProSu CNRS project for the financial support.

Appendix A. Supplementary data

Supplementary data associated with this article can be found, in the online version, at http://dx.doi.org/10.1016/j.cattod.2012.04.046.

References

[1] H.A. Gasteiger, W. Gu, R. Makharia, M.F. Mathias, B. Sompalli, Beginning-of-life MEA performance: efficiency loss contributions, in: W. Vielstich, A. Lamm, H.A. Gasteiger (Eds.), Handbook of Fuel Cells—Fundamentals, Technology, Applications, vol. 3, Wiley, Chichester, UK, 2003, p. 593.
[2] H.A. Gasteiger, S.S. Kocha, B. Sompally, F.T. Wagner, Applied Catalysis B 56 (2005) 9–35.
[3] B. Genorio, D. Strmcnik, R. Subbaraman, D. Tripkovic, G. Karapetrov, V.R. Stamenkovic, S. Pejovnik, N.M. Markovic, Nature Materials 9 (2010) 998–1003.
[4] M.B. Vukmirovic, J. Zhang, K. Sasaki, A.U. Nilekar, F. Uribe, M. Mavrikakis, R.R. Adzic, Electrochimica Acta 52 (2007) 2257–2263.
[5] L.N. Nekrasov, L. Muller, Doklady Akademii Nauk SSSR 149 (1963) 1107.
[6] A. Damjanovic, M.A. Genshaw, J.O'M. Bockris, Journal of the Electrochemical Society 114 (1967) 107–112.
[7] A. Damjanovic, M.A. Genshaw, J.O'M. Bockris, Journal of Electroanalytical Chemistry 15 (1973) 173–180.
[8] D. Dobos, Electrochemical Data, Akademiai Kiado, Budapesht, 1978.
[9] M. Savy, Electrochimica Acta 3 (1968) 1359–1376.
[10] R.H. Burshtein, V.S. Vilinskaya, M.R. Tarasevich, N.G. Bulavina, Reaction Kinetics and Catalysis Letters 4 (1976) 159–165.
[11] V.S. Bagotsky, N.A. Shumilova, E.I. Khrushcheva, Electrochimica Acta 21 (1976) 919.
[12] K. Kinoshita, Carbon—Electrochemical and Physicochemical Properties, Wiley, New York, USA, 1988.
[13] C. Song, J. Zhang, 2. Electrocatalytic oxygen reduction reaction, in: J. Zhang (Ed.), PEM Fuel Cell Electrocatalysts and Catalyst Layers: Fundamentals and Applications, Springer, 2008, pp. 89–134.
[14] J.B. Goodenough, Reports on Progress in Physics 67 (2004) 1915–1993.
[15] M.A. Pena, J.L.G. Fierro, Chemical Reviews 101 (2001) 1981–2017.
[16] A. Hammouche, A. Kahoul, D.U. Sauer, R.W. De Doncker, Journal of Power Sources 153 (2006) 239–244.
[17] J.O'M. Bockris, T. Otagawa, Journal of Physical Chemistry 87 (1983) 2960–2971.
[18] J. Tulloch, S. Donne, Journal of Power Sources 188 (2009) 359–366.
[19] R.N. Singh, M. Malviya, Anindita, A.S.K. Sinha, P. Chartier, Electrochimica Acta 52 (2007) 4264–4271.
[20] B.M. Ferreira, M.E. Melo Jorge, M.E. Lopes, M.R. Nunes, M.I. da Silva Pereira, Electrochimica Acta 54 (2009) 5902–5908.
[21] M. Hayashi, H. Uemura, K. Shimanoe, N. Miura, N. Yamazoe, Journal of the Electrochemical Society 151 (2004) A158–A163.
[22] J.P. Lukaszewicz, S. Imaizumi, M. Yuasa, K. Shimanoe, N. Yamazoe, Journal of Materials Science 41 (2004) 6215–6220.
[23] D. Thiele, A. Züttel, Journal of Power Sources 183 (2008) 590–594.
[24] S.-W. Eom, S.-Y. Ahn, I.-J. Kim, Y.-K. Sun, H.-S. Kim, Journal of Electroceramics 23 (2009) 382–386.
[25] M. Bursell, M. Pirjamali, Y. Kiros, Electrochimica Acta 47 (2002) 1651–1660.
[26] V. Hermann, D. Dutriat, S. Müller, Ch. Comninellis, Electrochimica Acta 46 (2000) 365–372.
[27] P. Wang, L. Yao, M. Wang, W. Wu, Journal of Alloys and Compounds 311 (2000) 53–56.
[28] J. Suntivich, H.A. Gasteiger, N. Yabuuchi, Y. Shao-Horn, Journal of The Electrochemical Society 157 (2010) B1263–B1268.
[29] J. Suntivich, H.A. Gasteiger, N. Yabuuchi, H. Nakanishi, J.B. Goodenough, Y. Shao-Horn, Nature Chemistry 3 (2011) 546–550.
[30] X. Li, W. Qu, J. Zhang, H. Wang, ECS Transactions 28 (2010) 45–56.
[31] H.-C. Yu, K.-Z. Fung, T.-C. Guo, W.-L. Chang, Electrochimica Acta 50 (2004) 811–816.
[32] J.O'M. Bockris, T. Otagawa, Journal of the Electrochemical Society 131 (1984) 290–302.
[33] A. Douy, International Journal of Inorganic Materials 3 (2001) 699–707.
[34] A.C. Larson, R.B. Von Dreele, General Structure Analysis System (GSAS), Los Alamos National Laboratory Report LA-UR-86-748, 2000.
[35] B.H. Toby, Journal of Applied Crystallography 34 (2001) 210–213.
[36] Y.I. Yermakov, V.F. Surovikin, G.V. Plaskin, V.A. Semikolenov, V.A. Likholobov, L.V. Chuvilin, S.V. Bogdanov, Reaction Kinetics and Catalysis Letters 33 (1987) 435–440.
[37] F. Maillard, P.A. Simonov, E.R. Savinova, 12. Carbon materials as supports for fuel cell electrocatalysts, in: P. Serp, J.L. Figueiredo (Eds.), Carbon Materials for Catalysis, Wiley, Hoboken, USA, 2008, pp. 429–480.
[38] V. Rao, P.A. Simonov, E.R. Savinova, G.V. Plaksin, S.V. Cherepanova, G.N. Kryukova, U. Stimming, Journal of Power Sources 145 (2005) 178–187.
[39] T.J. Schmidt, H.A. Gasteiger, G.D. Stäb, P.M. Urban, D.M. Kolb, R.J. Behm, Electrochemical Society Journal 145 (1998) 2354–2358.
[40] L.A. Tikhonova, G.I. Samal, P.P. Zhuk, A.A. Tonoyan, A.A. Vecher, Neorganicheskie Materialy 26 (1990) 184.
[41] F. Li, J.-F. Li, Ceramics International 37 (2011) 105–110.
[42] M. Cherry, M.S. Islam, C.R.A. Catlow, Journal of Solid State Chemistry 118 (1995) 125–132.
[43] M.S. Islam, M. Cherry, C.R.A. Catlow, Journal of Solid State Chemistry 124 (1996) 230–237.
[44] K. Tammeveski, K. Kontturi, R.J. Nichols, R.J. Potter, D.J. Schiffrin, Journal of Electroanalytical Chemistry 515 (2001) 101–112.
[45] U.A. Paulus, T.J. Schmidt, H.A. Gasteiger, R.J. Behm, Journal of Electroanalytical Chemistry 495 (2001) 134–145.
[46] P.S. Ruvinskiy, A. Bonnefont, M. Houllé, C. Pham-Huu, E.R. Savinova, Electrochimica Acta 55 (2010) 3245–3256.
[47] Q. Dong, S. Santhanagopalan, R.E. White, Journal of The Electrochemical Society 154 (2007) A888–A899.
[48] Y.N. Lee, R.M. Lago, J.L.G. Fierro, J. Gonzalez, Applied Catalysis A 215 (2001) 245–256.
[49] H. Falcon, R.E. Carbonio, J.L. Fierro, Journal of Catalysis 203 (2001) 264–272.
[50] A. Ariafard, H.R. Aghabozorg, F. Salehirad, Catalysis Communications 4 (2003) 561–566.
[51] Y. Matsumoto, H. Yoneyama, H. Tamura, Bulletin of the Chemical Society of Japan 51 (1978) 1927–1930.
[52] F. Jaouen, Journal of Physical Chemistry C 113 (2009) 15433–15443.
[53] A. Kahoul, A. Hammouche, F. Naamoune, P. Chartier, G. Poillerat, J.F. Koenig, Materials Research Bulletin 35 (2000) 1955–1966.
[54] W. Sun, A. Hsu, R. Chen, Journal of Power Sources 196 (2011) 627–635.
[55] F. Gloaguen, F. Andolfatto, R. Durand, P. Ozil, Journal of Applied Electrochemistry 24 (1994) 863–869.